Zitierweise: *Angew. Chem. Int. Ed.* **2024**, *63*, e202317435
doi.org/10.1002/anie.202317435

Gas Separation

Inverse Adsorption Separation of N_2O/CO_2 in AgZK-5 Zeolite

Li Wang, Caihong Lin, István Boldog, Jiangfeng Yang, Christoph Janiak,* and Jinping Li**

Abstract: Nitrous oxide (N_2O), as the third largest greenhouse gas in the world, also has great applications in daily life and industrial production, like anesthetic, foaming agent, combustion supporting agent, N or O atomic donor. The capture of N_2O in adipic acid tail gas is of great significance but remains challenging due to the similarity with CO_2 in molecular size and physical properties. Herein, the influence of cation types on CO_2–N_2O separation in zeolite was studied comprehensively. In particular, the inverse adsorption of CO_2–N_2O was achieved by AgZK-5, which preferentially adsorbs N_2O over CO_2, making it capable of trapping N_2O from an N_2O/CO_2 mixture. AgZK-5 shows a recorded N_2O/CO_2 selectivity of 2.2, and the breakthrough experiment indicates excellent performance for N_2O/CO_2 separation. The density functional theory (DFT) calculation shows that Ag^+ has stronger adsorption energy with N_2O, and the kinetics of N_2O is slightly faster than that of CO_2 on AgZK-5.

As the third largest greenhouse gas after carbon dioxide (CO_2) and methane (CH_4), nitrous oxide (N_2O) with a global warming potential (GWP) of about 300 causes a 300 times higher greenhouse effect than CO_2 and the concentration in the atmosphere has reached 333.2 ± 0.1 ppb in 2020.[1] It is worth noting that N_2O is also a valuable chemical which can be used as anesthetic, foaming agent, combustion supporting agent, N or O atomic donor, etc.[2] About 40 % of total N_2O emissions come from human activities, which arise from agriculture, transportation and industrial activities.[3] Industrially, N_2O is emitted as a by-product in the production of adipic acid. At present, thermal decomposition, catalytic decomposition and oxidation of benzene to phenol were used for the removal of N_2O.[4] However, these processes not only cause secondary pollution and high energy consumption but also waste the N_2O resources. Therefore, finding a cost-effective method to separate or enrich N_2O for other industrial applications is urgent and meaningful.

Particularly worth mentioning is that in addition to N_2O whose mass fraction is 38.4 wt % in adipic acid tail gas, CO_2 (6.1 wt %), N_2 (47.7 wt %), O_2 (5.6 wt %), H_2O (1.7 wt %), CO (0.3 wt %) and NO_2 (0.2 wt %) also exist in the tail gas, which shows that it is a big challenge to capture N_2O from this mixed tail gas.[5] Pressure swing adsorption (PSA) technology based on porous adsorbents catches a lot of attention in recent years because of its simple operation and low energy consumption.[6] For most adsorbents, the adsorption uptake order is H_2O or $NO_2 > CO_2$ or $N_2O > CO > N_2$ or O_2.[7] The mass contents of H_2O, CO and NO_2 are trace amounts and the physical properties are quite different from N_2O, so they are easy to remove upfront. Therefore, the $CO_2/N_2O/N_2/O_2$ mixture separation is the most important problem to be solved.

The physical property difference of N_2O towards N_2 and O_2 is obvious, so it is easy to separate.[7c,8] However, the molecular weight of CO_2 is 44 g/mol which is the same as the isoelectronic N_2O, also they are both linear molecules with a dynamic diameter of 3.3 Å. In addition, the boiling point (CO_2: 194.7 K; N_2O: 184.7 K) and polarizability (CO_2: $29.1\times10^{25}/cm^3$; N_2O: $30.3\times10^{25}/cm^3$) are very similar.[8b] In conclusion, the CO_2-N_2O separation is a great challenge for the selection of adsorbent. If CO_2 is removed first, two steps are needed to separate N_2O: CO_2/N_2O and then the N_2O/N_2 or O_2 separation. Obviously, the most important challenge is the mixture of CO_2/N_2O. So far, CO_2/N_2O separation can be effectively achieved by modifying MIL-100Cr with ethylenediamine and by regulating cations in zeolites.[9] However, if N_2O is directly preferentially adsorbed, high purity N_2O can be obtained by just one step. Thus, the most important aspect is the separation of N_2O/CO_2, which is simpler and more energy-saving, but the requirements for adsorbents are more stringent. For the separation of N_2O/CO_2, some flexible metal–organic frameworks (MOFs) can achieve preferential adsorption of N_2O, but the separation is not very efficient.[5,10] MIL-101Cr-NH_2 and MIL-100Fe with exposed Fe^{2+} unsaturated metal sites after high temperature and high vacuum activation can achieve preferential adsorption of N_2O and effective separation of N_2O/CO_2, but the selectivity is lower than 2.[7e,f] To this end, it is still very important to find an adsorbent with higher selectivity for N_2O.

As an important means to change the character of zeolite, ion exchange has a great influence on the adsorption and separation properties.[7d,11] Ag^+ exchanged zeolites and

[*] Dr. L. Wang, C. Lin, Prof. J. Yang, Prof. J. Li
College of Chemical Engineering and Technology, Taiyuan University of Technology
Taiyuan, 030024 Shanxi (China)
E-mail: yangjiangfeng@tyut.edu.cn
jpli211@hotmail.com
Dr. I. Boldog, Prof. C. Janiak
Institut für Anorganische Chemie und Strukturchemie, Heinrich-Heine-Universität Düsseldorf
40225 Düsseldorf (Germany)
E-mail: janiak@uni-duesseldorf.de
Prof. J. Yang, Prof. J. Li
State Key Laboratory of Clean and Efficient Coal Utilization, Taiyuan University of Technology
Taiyuan, 030024 Shanxi (China)

loaded MOFs materials have been researched widely for the separation of olefin from paraffin as Ag^+ is capable of π-complexation with olefins.[12] Also, Ag^+ exchanged zeolites can achieve efficient hydrogen isotope separation and N_2/CH_4 separation.[13] In the hard-soft-acid-base concept, CO_2 and N_2O possess quite similar moderate chemical hardness as Lewis bases (8.8 and 7.6 eV, respectively).[14] Ag^+ is a soft Lewis acid with chemical hardness of 6.96 eV and N_2O is a slightly softer Lewis base as compared to CO_2, so N_2O may have a stronger interaction with Ag^+.

In this work, the adsorption and separation performance of CO_2 and N_2O on Ag^+ exchanged 8-membered ring KFI-type zeolite ZK-5 was studied. Compared with the original zeolite KZK-5, the modified zeolite AgZK-5 achieved adsorption reversal, from CO_2-selective adsorbent to N_2O-selective adsorbent.

The KFI structure contains 8-hedral double 6-rings (d6rs), 18-hedral pau cages, and 26-hedral lta cages, wherein the window size of its 8-ring is 3.9×3.9 Å which is suitable for N_2O and CO_2 molecular adsorption (Figure S1).[15] Powder X-ray diffraction (PXRD) confirmed that the structures of AgZK-5 are maintained well compared with the original zeolites (Figures S2–3). The content and homogeneous distribution of silver were confirmed by inductively coupled plasma-optical emission spectroscopy (ICP-OES, Tables S1–3) and energy dispersive spectrum (EDS, Figures S4–6). The water molecules in the pore of AgZK-5 could be removed completely by heating to 523 K (Figures S7–8). The N_2 adsorption capacity at 77 K and Brunauer–Emmett–Teller (BET) surface area of ZK-5 zeolite changes from 85 cm^3/g to 123 cm^3/g and 298 m^2/g to 434 m^2/g respectively after K^+ is exchanged with Ag^+ (Table S4 and Figures S9–11), due to the smaller size of Ag^+ than K^+ (radius Ag^+: 1.15 Å, K^+: 1.38 Å).

The state of silver was confirmed by X-ray photoelectron spectroscopy (XPS) and ultraviolet and visible spectrophotometry (UV/Vis), and all of them indicate that silver exists mainly in the state of monovalent silver in the zeolites (Figures S12–15).[16] However, those methods, particularly XPS, detect silver only on in the surface layer. In order to assess the average localization of silver thorough the sample, Rietveld refinement of powder X-ray diffraction data was attempted. A preliminary check confirmed the data consistency via Le Bail fitting (Figure S16), which showed that the AgZK-5 is nearly phase-pure and retains almost precisely the unit cell parameters ($Im\bar{3}m$, 18.686 Å vs 18.578 Å for ZK-5). The Rietveld refinement (Figure S17, Bragg R = 11.7 %) suggests seven Ag locations (Tables S5–6), with three of them representing the major silver content (Figures S18d and S19–25): Ag1, somewhat out of the 8-membered ring plane towards the center the spherical pore (Figure S18a); Ag2, slightly offset from the planes of the double 6-membered ring, and delocalized over three close positions related by a 3 axis (Figure S18b); and Ag3, close to the interior of the spherical cavity (Figure S18c). It is important to note that the Rietveld refinement gives only a quite approximate silver atoms positions, which is reflected by the high refined thermal displacement factor (in other words, the most probable localizations of the Ag atoms are not confined to small areas, but covers significant volumes). As for the nature of those silver atoms, Ag2 unambiguously represents Ag^+ ions, Ag3 represents small silver clusters randomly scattered in the pores, and Ag1 could represent both. The primary location of confined K^+ and Ag^+ sites in ZK-5 zeolite were also studied by density functional theory (DFT) calculations, as shown in Figures 1 and S26. Both K^+ and Ag^+ have the lowest energy out of the 8-membered ring plane of ZK-5, which is 0.00 eV, indicating that K^+ and Ag^+ are most stable in this location. However, the Rietveld refinement strongly suggests that there are delocalized silver clusters closer to the center of the pores. The DFT calculations not explicitly accounts for those clusters, but focuses on the localization of the single-atom Ag sites, which are assumed to be the catalytically most productive ones (corresponds primarily to Ag2 in the refined structure).

To evaluate the separation potential of Ag^+ exchanged zeolites for CO_2 and N_2O, single-component adsorption isotherms for CO_2, N_2O and N_2 on parent and Ag^+ exchanged zeolites were collected at 298 K and 1 bar (Figures 2a–c and S27–29). Clearly, before the Ag^+ exchange, CO_2 adsorption capacities on KZK-5, NaX and KChabazite exceed the capacity of N_2O, indicating a CO_2-selective property and the CO_2/N_2O selectivity at 298 K and1 bar are calculated by ideal adsorbed solution theory (IAST) after fitted by the dual-site Langmuir equation, which are 2.2, 2.1 and 3.0, respectively (Figure 2d, S37 and Table S7). The fitting curves and parameters are shown in Figures S30–32, S36 and Tables S8 and S11. Interestingly, after the Ag^+ exchange, the adsorption capacity of CO_2 and N_2O was inverted on AgZK-5, AgX and AgChabazite. Specifically, the adsorption capacity of N_2O became higher than that of CO_2 in Ag-zeolites. Thus, after the Ag^+ exchange the modified zeolites AgZK-5, AgX and AgChabazite represent N_2O-selective adsorbents and their N_2O/

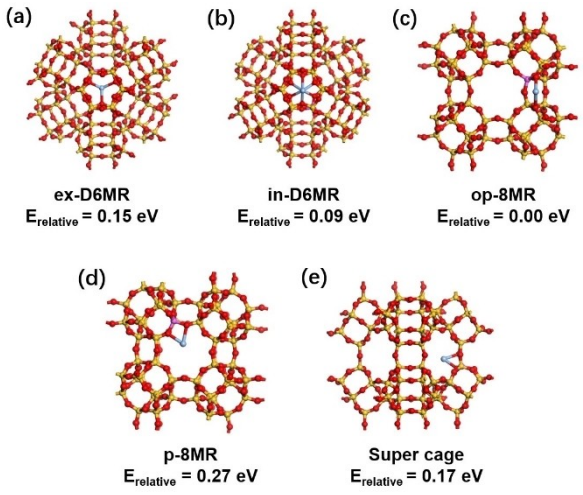

Figure 1. Relative energies of Ag + in different positions of ZK-5 zeolite: (a) Ag + in the exterior of the double 6-membered ring, (b) Ag + in the interior of the double 6-membered ring, (c) Ag + out of the 8-membered ring plane, (d) Ag + in the 8-membered ring plane and (e) Ag + in the super cage. (O: red, Si: yellow, Al: pink and Ag: light blue)

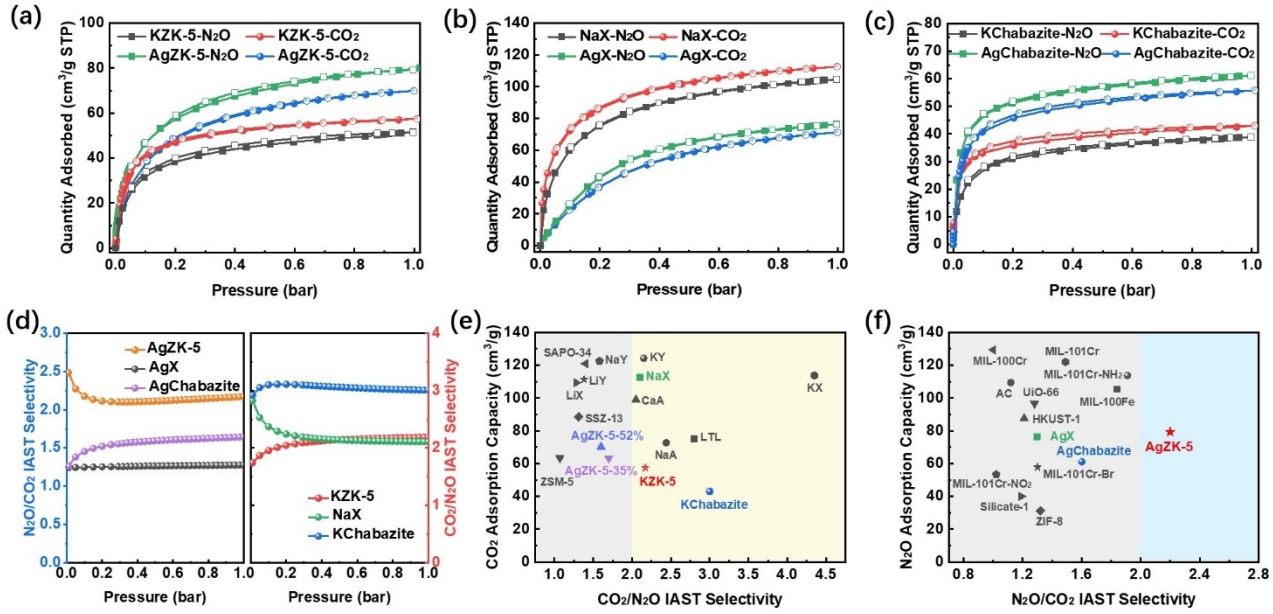

Figure 2. CO_2 and N_2O sorption isotherms at 298 K on (a) KZK-5 and AgZK-5, (b) NaX and AgX, (c) KChabazite and AgChabazite (filled symbols adsorption, empty symbols desorption), (d) IAST selectivity of CO_2/N_2O or N_2O/CO_2 on different zeolite with different cations, (e) CO_2/N_2O adsorption selectivity plotted against CO_2 uptake at 298 K and 1 bar for some benchmark adsorbents and (f) N_2O/CO_2 adsorption selectivity plotted against N_2O uptake at 298 K and 1 bar for some benchmark adsorbents.

CO_2 selectivity at 298 K and 1 bar are 2.2, 1.2 and 1.6, respectively. In addition, N_2O can be good desorption, indicating no decomposition of N_2O upon the adsorption process. It is worth noting that when the degree of Ag^+ exchange in ZK-5 is 35 % and 52 % (AgZK-5–35 % and AgZK-5–52 %), the modified ZK-5 zeolites are still CO_2-selective adsorbents (Figure S33), but CO_2/N_2O selectivity decreases from 2.2 to 1.6 (Figure S34). This shows that the adsorption reversal of CO_2-N_2O can be realized only when the exchange degree reaches a certain level. ZK-5 with different cations have different adsorption separation properties. When the cation is K^+, KZK-5 shows preferable CO_2/N_2O selectivity and when the cation is Ag^+, AgZK-5 exhibits high N_2O/CO_2 selectivity (record data) as shown in Figures 2e–f and Tables S9–10, indicating an excellent adsorbent for the separation of CO_2–N_2O binary mixture, especially the separation of N_2O/CO_2. The adsorption heats of N_2O and CO_2 on KZK-5 and AgZK-5 were calculated by the virial equation using the 298 K, 308 K and 318 K adsorption isotherms (Figures S35 and S38–39), which changes from $Q_{st(CO2)} > Q_{st(N2O)}$ on original zeolite to $Q_{st(N2O)} > Q_{st(CO2)}$ on Ag^+ exchanged zeolite (Figure S40). The desorption peak of N_2O on temperature-programmed desorption (TPD) was observed in the temperature range of 40–200 °C, indicating the complete regeneration of these zeolites upon thermal treatment at 200 °C or higher (Figures S41–43). In situ Fourier transform infrared spectra (In situ FTIR) with the gradual increase of N_2O flow indicates N_2O is successfully adsorbed on AgZK-5, and the adsorbed N_2O increases gradually with the increase of flow rate (Figures S44–46).

To understand the above reverse adsorption phenomenon in more detail, the adsorption energies of CO_2 and N_2O with K^+ and Ag^+ located out of the 8-membered ring plane (Ag1) and exterior of the double 6-membered ring (Ag2) were calculated (Figures 3 and S47–48). The adsorption energies of K^+ with CO_2 and N_2O (N end) on Ag1 are −0.47 eV and −0.48 eV, showing that K^+ has a similar

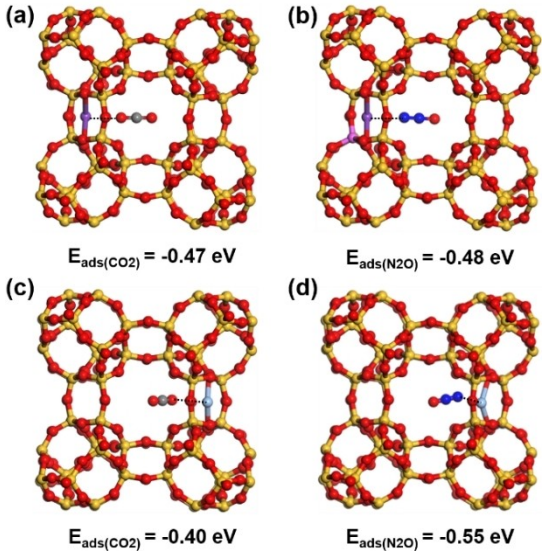

Figure 3. Adsorption energies of CO_2 and N_2O on ZK-5 with different cations: (a) K^+–CO_2, (b) K^+–N_2O, (c) Ag^+–CO_2 and (d) Ag^+–N_2O. (O: red, Si: yellow, C: grey, N: dark blue, Ag: light blue, K: purple)

interaction force with CO_2 and N_2O (Figures 3a and 3b). However, when the original cation (K^+/Na^+) was exchanged by Ag^+, the adsorption energy shows a remarkable difference. The adsorption energy of Ag^+ with CO_2 and N_2O (N end) are −0.40 eV and −0.55 eV, respectively (Figures 3c and 3d), indicating that Ag^+ has a stronger interaction with N_2O than CO_2, which is in accordant with the above mentioned N_2O-selective adsorption material after Ag^+ exchange. In order to further verify that Ag^+ interacts with N_2O through N end, in situ FTIR of N_2O and Ag^+–N–N–O or K^+– N–N–O in ZK-5 were simulated (Figure S49). Results show that when N_2O is adsorbed on the zeolites, the wavelength of N_2O shifts towards to the long wavelength, from 2347 cm^{-1} of N_2O to 2387 cm^{-1} of Ag^+–N–N–O in ZK-5, which is consistent with the experiment result, proving N_2O interacts with Ag^+ through the N end.[17]

The gas diffusion kinetic data of ZK-5 with different cations were collected on an intelligent gravimetric analyzer (Hiden IGA 001). For KZK-5, CO_2 reaches equilibrium slightly faster than N_2O (CO_2: ca. 23 min; N_2O: ca. 42 min), which explains the reason for CO_2-selective adsorption on KZK-5. (Figure 4a). Notably, the time to reach the equilibrium of N_2O on AgZK-5 is shorter than for CO_2 (N_2O: ca. 8 min; CO_2: ca. 10.5 min), which is consistent with the adsorption data and DFT calculated result.

These excellent results for equilibrium and kinetic adsorption encouraged us to further evaluate the performance of AgZK-5 in the N_2O/CO_2 separation process. The samples were pressed and granulated, with almost no adsorption loss (Figures S50–51). Breakthrough experiments were carried out using a fixed bed packed with different zeolites pellets at 298 K and a total inlet pressure of 1 bar with a N_2O/CO_2 mixture (50 %/50 %, v/v) as the feed gas. The original zeolites KZK-5, NaX and KChabazite are all excellent CO_2 selective adsorbents with N_2O showing preferential breakthrough through the adsorption column (Figures 4b and S52–54). After Ag^+ exchange, N_2O is preferentially adsorbed on Ag-zeolites and the CO_2 breakthrough time is earlier than N_2O (Figures 4c and S55–56). The breakthrough curves of AgZK-5 with different flow are shown in Figure 4c. The results shows that the retention time (retention time = N_2O breakthrough time minus CO_2 breakthrough time) and R (R = retention time/CO_2 breakthrough time) increase with the increase of the gas flow rate from 8 mL/min to 15 mL/min (Figure 4d). When the gas flow rate is 15 mL/min, the retention time and R reach the maximum, which are 3 min and 0.11 respectively, indicating that AgZK-5 has the best separation performance at 15 mL/min. When the gas flow rate reaches 20 mL/min, the retention time and R decrease sharply. Finally, the adsorption and desorption cycle experiments, PXRD after pelleting and adsorption and the breakthrough experiment of another batch AgZK-5 show that it has a good stability which can meet the demand in a real process (Figures 4e and S57–58).

In summary, an unprecedented N_2O/CO_2 separation strategy has been developed, based on Ag^+ exchanged zeolites. Efficient separation of N_2O/CO_2 was achieved due to the stronger interaction of N_2O with the Ag^+ cation within the zeolite micropores and the dynamics of N_2O is faster than CO_2 on AgZK-5. To the best of our knowledge, the obtained AgZK-5 exhibits the highest N_2O/CO_2 selectivity hitherto recorded among adsorbents. Breakthrough experiments demonstrated that N_2O could be efficiently separated from a N_2O/CO_2 (50:50, v/v) mixture at a flow of

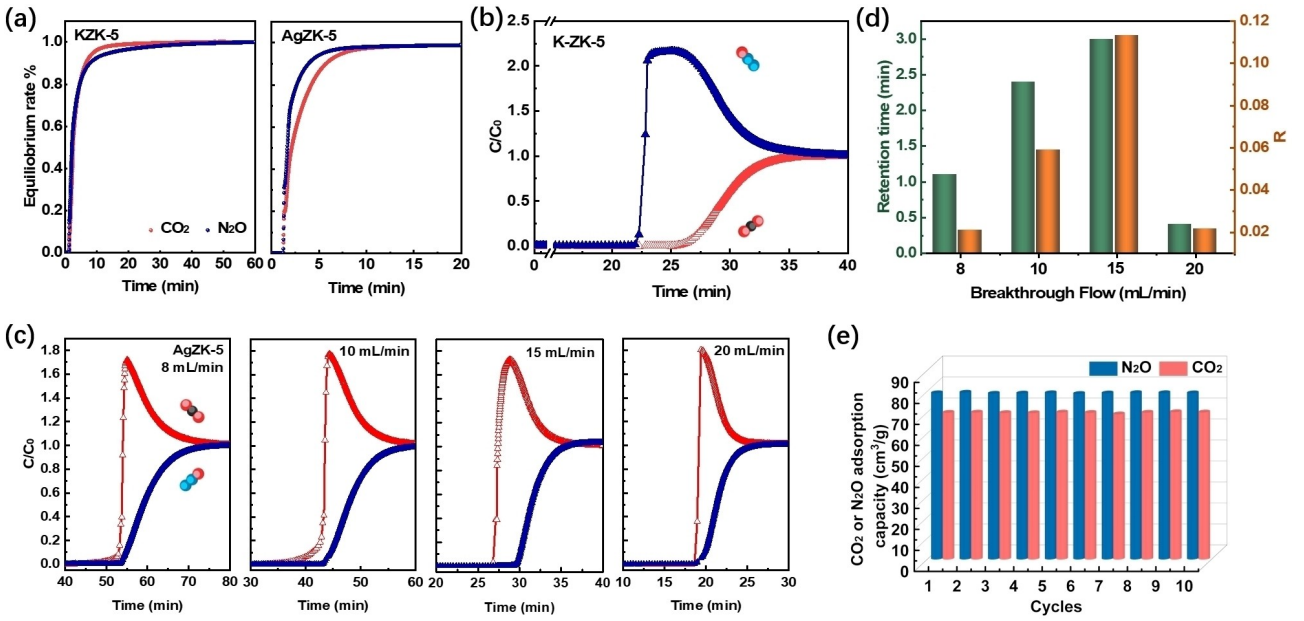

Figure 4. (a) Kinetic curves of CO_2 and N_2O on KZK-5 and AgZK-5. (b) Breakthrough curve of a CO_2/N_2O mixture (50%/50%) on KZK-5 at 15 mL/min. (c) Breakthrough curves of a N_2O/CO_2 mixture (50%/50%) with different flow on AgZK-5. (d) Comparison of retention time and R (R = retention time/CO_2 breakthrough time) on AgZK-5 with different breakthrough flow and (e) comparison of cyclic N_2O and CO_2 adsorption capacity on AgZK-5.

15 mL/min. The realization of this strategy provides a high-performance adsorbent for industrial N_2O enrichment.

Acknowledgements

We acknowledge the financial support from the National Natural Science Foundation of China (No. 22308238 and 22378287).

Conflict of Interest

The authors declare no conflict of interest.

Data Availability Statement

The data that support the findings of this study are available in the supplementary material of this article.

Keywords: Adsorption Inversion · Ag^+ Exchanged Zeolites · N_2O/CO_2 Separation · ZK-5

[1] a) J. Ephraums, G. Jenkins, Cambridge University Press, **1992**; b) D. A. Lashof, D. R. Ahuja, *Nature* **1990**, *344*, 529–531; c) D. J. Wuebbles, *Science* **2009**, *326*, 56–57; d) A. Ravishankara, J. S. Daniel, R. W. Portmann, *Science* **2009**, *326*, 123–125.

[2] a) D. J. Xiao, E. D. Bloch, J. A. Mason, W. L. Queen, M. R. Hudson, N. Planas, J. Borycz, A. L. Dzubak, P. Verma, K. Lee, *Nat. Chem.* **2014**, *6*, 590–595; b) M. Konsolakis, *ACS Catal.* **2015**, *5*, 6397–6421; c) K. Severin, *Chem. Soc. Rev.* **2015**, *44*, 6375–6386; d) Y. Wang, M. Chen, Y. Xie, P. Wei, H. F. Schaefer, P. Schleyer, G. H. Robinson, *Nat. Chem.* **2015**, *7*, 509–513; e) S. Saito, H. Ohtake, N. Umezawa, Y. Kobayashi, N. Kato, M. Hirobe, T. Higuchi, *Chem. Commun.* **2013**, *49*, 8979–8981; f) J. J. Chen, H. M. Huang, *Nat. Chem.* **2022**, *14*, 846–848.

[3] a) D. S. Reay, E. A. Davidson, K. A. Smith, P. Smith, J. M. Melillo, F. Dentener, P. J. Crutzen, *Nat. Clim. Change* **2012**, *2*, 410–416; b) Z. Hu, J. W. Lee, K. Chandran, S. Kim, S. K. Khanal, *Environ. Sci. Technol.* **2012**, *46*, 6470–6480.

[4] a) X. Xu, H. Xu, F. Kapteijn, J. A. Moulijn, *Appl. Catal. B* **2004**, *53*, 265–274; b) F. Zhang, X. Chen, J. Zhuang, Q. Xiao, Y. Zhong, W. Zhu, *Catal. Sci. Technol.* **2011**, *1*, 1250–1255; c) F. Le Vaillant, A. Mateos Calbet, S. Gonzalez-Pelayo, E. J. Reijerse, S. Ni, J. Busch, J. Cornella, *Nature* **2022**, *604*, 677–683; d) J. Pérez-Ramírez, F. Kapteijn, K. Schöffel, J. A. Moulijn, *Appl. Catal. B* **2003**, *44*, 117–151.

[5] D.-L. Chen, N. Wang, F.-F. Wang, J. Xie, Y. Zhong, W. Zhu, J. K. Johnson, R. Krishna, *J. Phys. Chem. C* **2014**, *118*, 17831–17837.

[6] C. A. Grande, F. Poplow, A. E. Rodrigues, *Sep. Sci. Technol.* **2010**, *45*, 1252–1259.

[7] a) K. Yamashita, Z. Liu, K. Iyoki, C. T. Chen, S. Miyagi, Y. Yanaba, Y. Yamauchi, T. Okubo, T. Wakihara, *Chem. Commun.* **2021**, *57*, 1312–1315; b) T. Wu, Y. Shen, L. Feng, Z. Tang, D. Zhang, *J. Chem. Eng. Data* **2019**, *64*, 3473–3482; c) X. Zhang, W. Chen, W. Shi, P. Cheng, *J. Mater. Chem. A* **2016**, *4*, 16198–16204; d) J. Yang, Q. Zhao, H. Xu, L. Li, J. Dong, J. Li, *J. Chem. Eng. Data* **2012**, *57*, 3701–3709; e) L. Wang, F. Zhang, J. Yang, L. Li, J. Li, *Chem. Commun.* **2021**, *57*, 6636–6639; f) L. Ma, F. Zhang, K. Li, Y. Zhang, Z. Song, L. Wang, J. Yang, J. Li, *J. Solid State Chem.* **2022**, *309*, 122951; g) J. Peng, S. Xian, J. Xiao, Y. Huang, Q. Xia, H. Wang, Z. Li, *Chem. Eng. J.* **2015**, *270*, 282–289; h) J. W. Yoon, Y. K. Seo, Y. K. Hwang, J. S. Chang, H. Leclerc, S. Wuttke, P. Bazin, A. Vimont, M. Daturi, E. Bloch, *Angew. Chem. Int. Ed.* **2010**, *49*, 5949–5952; i) J. Li, Z. Wang, Y. Chen, Y. Cheng, L. L. Daemen, F. Tuna, E. J. L. McInnes, S. J. Day, A. J. Ramirez-Cuesta, M. Schroder, S. Yang, *J. Am. Chem. Soc.* **2022**, *144*, 18967–18975; j) Y. X. Li, W. Zhong, J. J. Zhou, S. C. Qi, X. Q. Liu, L. B. Sun, *Angew. Chem. Int. Ed.* **2022**, *61*, e202212732.

[8] a) J. Yang, B. Du, J. Liu, R. Krishna, F. Zhang, W. Zhou, Y. Wang, J. Li, B. Chen, *Chem. Commun.* **2018**, *54*, 14061–14064; b) J. R. Li, R. J. Kuppler, H. C. Zhou, *Chem. Soc. Rev.* **2009**, *38*, 1477–1504.

[9] a) L. Wang, F. Zhang, C. Wang, Y. Li, J. Yang, L. Li, J. Li, *Sep. Purif. Technol.* **2020**, *235*, 116219; b) L. Wang, J. Liu, C. Lin, H. Shang, J. Yang, L. Li, J. Li, *Chem. Eng. J.* **2022**, *431*,134257.

[10] L. Wang, Y. Li, Y. Wang, J. Yang, L. Li, J. Li, *Sep. Purif. Technol.* **2020**, *251*, 117311.

[11] a) A. Primo, H. Garcia, *Chem. Soc. Rev.* **2014**, *43*, 7548–7561; b) V. J. Inglezakis, M. M. Loizidou, H. P. Grigoropoulou, *J. Colloid Interface Sci.* **2004**, *275*, 570–576; c) F. E. Epiepang, X. Yang, J. Li, Y. Liu, R. T. Yang, *AIChE J.* **2018**, *64*, 406–415; d) M. L. Zanota, N. Heymans, F. Gilles, B. L. Su, G. De Weireld, *Microporous Mesoporous Mater.* **2011**, *143*, 302–310.

[12] a) S. Aguado, G. Bergeret, C. Daniel, D. Farrusseng, *J. Am. Chem. Soc.* **2012**, *134*, 14635–14637; b) Y. Xiong, T. Tian, A. L′Hermitte, A. S. J. Méndez, D. Danaci, A. E. Platero-Prats, C. Petit, *Chem. Eng. J.* **2022**, *446*, 137104.

[13] a) L. Zhang, T. Wulf, F. Baum, W. Schmidt, T. Heine, M. Hirscher, *Inorg. Chem.* **2022**, *61*, 9413–9420; b) D. A. Kennedy, M. Khanafer, F. H. Tezel, *Microporous Mesoporous Mater.* **2019**, *281*, 123–133; c) X. Hao, H. Hu, Z. Li, L. Wu, X. Liu, Y. Zhang, *Materials* **2018**, *11*, 2024.

[14] R. G. Pearson, *Inorg. Chem.* **1988**, *27*, 734–740.

[15] C. Baerlocher, http://www. iza-structure. org/databases/2008. (The web page was accessed November 16, 2022.).

[16] J. G. Min, K. C. Kemp, S. B. Hong, *Sep. Purif. Technol.* **2020**, *250*, 117146.

[17] a) N. U. Zhanpeisov, G. Martra, W. S. Ju, M. Matsuoka, S. Coluccia, M. Anpo, *J. Mol. Catal. A* **2003**, *201*, 237–246; b) W. B. Tolman, *Angew. Chem. Int. Ed.* **2010**, *49*, 1018–1024.

Manuscript received: November 15, 2023
Accepted manuscript online: December 7, 2023
Version of record online: December 20, 2023